# Numerical simulations of upstream and downstream overdeepening

## Carina VAN DER MEER

Delft University of Technology, Faculty of Civil Engineering, Delft, the Netherlands

## Erik MOSSELMAN, Kees C. J. SLOFF

Deltares, Delft, the Netherlands

Delft University of Technology, Faculty of Civil Engineering, Delft, the Netherlands

### Bert JAGERS

Deltares, Delft, the Netherlands

## Guido ZOLEZZI, Marco TUBINO

University of Trento, Trento, Italy

ABSTRACT: Local geometrical perturbations of alluvial channels can generate a pattern of non-migrating bars and pools. This phenomenon is known as "overdeepening", because the pools locally enhance the scour in river bends. Overdeepening occurs only downstream of a perturbation if the channel is in the subresonant and subcritically damped regime, which corresponds to channels with moderate width-to-depth ratios. Previous theoretical analyses and laboratory experiments show that overdeepening occurs also upstream of geometrical perturbations in the relatively wide channels of the superresonant regime (Zolezzi & Seminara, 2001; Zolezzi et al, 2005; Mosselman et al, 2006). We use a two-dimensional depth-averaged morphological model to explore the occurrence of upstream and downstream overdeepening numerically. The simulations reproduce the overall picture arising from previous theoretical and experimental findings. Non-migrating bars and pools appear downstream of perturbations if the regime is subresonant. The bar pattern appears both upstream and downstream if the regime is superresonant. However, two findings in the computational results differ from linear theory. First, the threshold between subresonant and superresonant regimes is higher in the numerical computations than predicted by linear theory. Second, at very high width-to-depth ratios in the superresonant regime, the computed non-migrating bars are shorter than predicted by linear theory (and observed experimentally). We explain the higher threshold from numerical diffusion, and the shorter bars from limited simulation duration, numerical diffusion and the non-linear effects suggested by Siviglia et al (2011).

#### 1 INTRODUCTION

Alluvial river beds often display typical patterns of shallow bars that occur alternately at the left and the right bank. Early work by Hansen (1967) and Callender (1969) showed that these alternate bars can be explained by a stability analysis of the mathematical equations for flow and sediment transport. Subsequent work led to the classical linear theories by Blondeaux & Seminara (1985) and Struiksma et al (1985). Hereafter we refer to these theories as "BS" and "SOFD", respectively. BS considers the general case of migrating bars in straight channels without geometrical perturbations and reveals that non-migrating bars arise as a special case of migrating bars under resonant conditions, i.e. conditions of vanishing damping. SOFD considers the case of non-migrating bars generated by a local geometrical

perturbation, such as a cross-dam closing part of the cross-section, or a discontinuity in channel curvature, such as the entrance or exit of a circular bend. Parker & Johanneson (1989) call the non-migrating bars of SOFD "overdeepening", because the associated non-migrating pools enhance the outer-bend scour that would occur in infinitely long bends where the system of flow and sediment transport is fully developed (axisymmetric case). Mosselman et al (2006) call these SOFD non-migrating bars "spatial bars". At the width-to-depth ratio of zero damping, these spatial bars are equal to the BS non-migrating bars arising at resonant conditions. Zolezzi & Seminara (2001) show that overdeepening occurs downstream of geometrical perturbations if the width-to-depth ratio is smaller than the resonant value (subresonant regime), but upstream of geometrical perturbations if the width-to-depth ratio is larger (superresonant regime). Laboratory experiments by Zolezzi et al (2005) showed that, indeed, overdeepening occurred only downstream under subresonant conditions, but both upstream and downstream under superresonant conditions. Here we present a numerical exploration of upstream and downstream overdeepening by using a fully nonlinear two-dimensional depth-averaged morphological model.

#### 2 THEORY

The models for alternate bars by BS and SOFD are based on physics-based depth-averaged equations for conservation of sediment mass, water mass and water flow momentum, along with a parameterization of 3D effects from curvature-induced helical flow and empirical closure relations linking hydraulic roughness and sediment transport to flow parameters and sediment properties. BS and SOFD both yield fourth-order linear models, but Struiksma et al (1985) also compare their fourth-order model with a strongly simplified second-order model, a comparison later revisited by Camporeale et al (2007). The second-order model appears to be a good approximation of the complete fourth-order model for (subcritically damped) subresonant conditions and the lower width-to-depth range of superresonant conditions. This justified the adoption of the second-order model in Crosato's (1989, 2008) meander model. BS uses a sediment transport formula of the type of Meyer-Peter & Müller (1948), whereas SOFD uses a formula of the type of Engelund & Hansen (1967). Furthermore, SOFD simplifies the relation for hydraulic roughness to a constant value independent of flow parameters and sediment properties. The closure relations for sediment transport regard not only the magnitude but also the direction of sediment transport. This direction can be given by

$$\tan \alpha_s = \frac{\sin \alpha_\tau - \frac{1}{f} \frac{\partial z_b}{\partial y}}{\cos \alpha_\tau - \frac{1}{f} \frac{\partial z_b}{\partial x}}$$
(1)

where  $\alpha_s$  is the direction of sediment transport,  $\alpha_r$  is the direction of bed shear stress,  $z_b$  is the bed level, x and y are longitudinal and transverse co-ordinates, respectively, and f is a non-dimensional parameter weighing the effect of gravity on the motion of sediment particles on sloping beds. The latter has been found to be proportional to the Shields mobility parameter,  $\theta$ :

$$f = \frac{1}{r}\sqrt{\theta} \tag{2}$$

where the non-dimensional coefficient, r, usually assumes a constant value through calibration, although it weakly depends on the ratio of sediment grain size to flow depth (Talmon et al, 1995).

The linear theories of BS and SOFD are similar and mutually consistent, but they differ in details, such as the empirical closure relations, and they have provided different yet complementary interpretations. Parker & Johanneson (1989) therefore distinguish a "Genova School" (Blondeaux, Seminara and co-workers) and a "Delft School" (Struiksma and co-workers). Another difference lies in the notations. BS and later improvements use non-dimensional quantities, thus emphasizing the generic mathematical character of the equations and the possible analogies with similar equations for other physical phenomena. SOFD and later improvements use dimensional quantities that are more easily recognized in engineering and geomorphological practice. Table 1 provides an overview. One of the peculiar consequences is that the BS

width-to-depth ratio,  $\beta$ , is half as large as the SOFD width-to-depth ratio, because BS scales horizontal co-ordinates with half the channel width. This scaling may be less intuitive for practicing engineers and geomorphologists, but leads to mathematically convenient and elegant bank-line locations at values +1 and -1 of the non-dimensional transverse co-ordinate, n.

Table 1 Conversion table for SOFD and BS notations

Description	Dimensiona	1 quantities	Non-dimensional quantities				
Description	SOFD	BS	SOFD	BS			
longitudinal co-ordinate	X	$s^*$	2x/B	$S = S^* / B^*$			
transverse co-ordinate	У	$n^*$	2y/B	$n=n^*/B^*$			
time	t	$t^*$	$2u_0t/B$	$t = U_0^* t^* / B^*$			
longitudinal flow velocity	и	$U^*$	$u/u_0$	$U = U^* / U_0^*$			
transverse flow velocity	v	$V^*$	$v/v_0$	$V = V^* / V_0^*$			
Froude number	-	-	$Fr = u / \sqrt{gh}$	$F = U / \sqrt{gD}$			
water level	$Z_w$	$h^*$	$z_w / (Fr_0^2 h_0)$	$H = h^* / \left(F_0^2 D_0^*\right)$			
flow depth	h	$D^*$	$h/h_0$	$D = D^* / D_0^*$			
channel width	B	$2B^*$	-	-			
width-to-depth ratio	-	-	$B/h_0$	$2\beta = 2B^* / D_0^*$			
sediment diameter	D	$d_s^*$	$D/h_0$	$d_s = d_s^* / D_0^*$			
hydraulic roughness	C	-	$g/C^2$	$C_f = 1/C^2$			
longitudinal bed shear stress	$ au_{bx}$	$ au_s^*$	$ au_{bx}/ig( ho u_0^2ig)$	$\tau_s = \tau_s^* / \left(\rho U_0^{*2}\right)$			
submerged sediment mass density	$\rho_s - \rho$	$\rho_s - \rho$	$\Delta = (\rho_s - \rho)/\rho$	$\rho_s/\rho-1$			
longitudinal sediment transport per unit width excluding pores	$(1-\varepsilon)s_x$	$Q_s^*$	$\frac{(1-\varepsilon)s_x}{D\sqrt{g\Delta D}}$	$Q_s = \frac{Q_s^*}{d_s^* \sqrt{g(\rho_s/\rho - 1)d_s^*}}$			

The BS linear theory shows evolution and pattern of alternate bars to be primarily governed by the width-to-depth ratio,  $\beta$ , and the non-dimensional bed shear stress (or Shields parameter for sediment mobility),  $\theta$ . For the strongly simplified second-order model, the SOFD linear theory combines these two main controlling factors into a single interaction parameter,  $\lambda_s / \lambda_w$ , defined as

$$\frac{\lambda_s}{\lambda_w} = \frac{2}{\pi^2} \frac{g}{C^2} \left(\frac{B}{h_0}\right)^2 \frac{\sqrt{\theta}}{r} = \frac{8}{\pi^2} \frac{g}{C^2} \beta^2 \frac{\sqrt{\theta}}{r}$$
(3)

where g is the acceleration due to gravity and C is the Chézy coefficient for hydraulic roughness. In the SOFD second-order model, the spatial damping length,  $L_D$ , and the bar wave length,  $L_P$ , are simple functions of the interaction parameter:

$$\frac{1}{L_D} = \frac{1}{2\lambda_w} \left( \frac{\lambda_w}{\lambda_s} - \frac{b - 3}{2} \right) \tag{4}$$

$$\frac{2\pi}{L_{P}} = \frac{1}{\lambda_{w}} \sqrt{\frac{\lambda_{w}}{\lambda_{c}} - \left(\frac{\lambda_{w}}{L_{D}}\right)^{2}} \tag{5}$$

where  $\lambda_w = (C^2/2g)h_0$ ,  $h_0$  is the reach-averaged flow depth and b denotes the degree of non-linearity

in the dependence of sediment transport on depth-averaged flow velocity (Mosselman, 2005).

The linear theories reveal key thresholds for  $\beta$  (and, equivalently,  $\lambda_s/\lambda_w$  and  $B/h_0$ ) that separate different regimes of bar behaviour. Firstly, a critical width-to-depth ratio,  $\beta_{cr}$ , separates narrower or deeper channels where free alternate bars are suppressed from wider or shallower channels where these bars can grow (Colombini et al, 1987). We emphasize that this threshold holds for free bars only, because spatial bars can occur at width-to-depth ratios both above and below  $\beta_{cr}$ . Secondly, a resonant width-to-depth ratio,  $\beta_{res}$ , separates narrower or deeper channels where free alternate bars migrate downstream from wider or shallower channels where these bars migrate upstream when their amplitude is small, consistent with the linear approximation. Zolezzi & Seminara (2001) predict theoretically that a geometrical perturbation produces spatial bars downstream of this perturbation if  $\beta < \beta_{res}$  (subresonant regime) and upstream if  $\beta > \beta_{res}$  (superresonant regime). Laboratory experiments by Zolezzi et al (2005) confirmed this prediction, but resulted in spatial bars both upstream and downstream for  $\beta > \beta_{res}$ , which was expected on the basis of an analysis of characteristics (Mosselman et al, 2006). The present paper addresses this upstream and downstream occurrence of spatial bars in subresonant and superresonant regimes numerically.

#### 3 METHOD

We used the Delft3D modelling system (Lesser et al, 2004) in 2D depth-averaged mode to compute the evolution of the bed in the 0.6 m wide laboratory flume of Zolezzi et al (2005). The longitudinal slope was 0.011 m/m and the Chézy coefficient 22.5 m<sup>1/2</sup>/s, leading to a Froude number of 0.75 in all simulations. The sediment grain size was equal to 1 mm. We varied the width-to-depth ratio and the Shields mobility parameter by varying the discharge, Q, imposed at the upstream boundary. For each computation, we set the downstream water level to a value which rendered the flow uniform without backwater effects. The upstream sediment supply was taken equal to the sediment transport capacity at the upstream boundary. We applied the sediment transport formula of Meyer-Peter & Müller (1948) with a constant ripple factor equal to 0.7. The effect of transverse bed slopes on the direction of sediment transport was represented by Equation (2) with f = 1/r = 1.9. The Delft3D calibration factor, ESPIR, for the effect of helical flow on the direction of bed shear stress was set at 0.5. We carried out 25 computations labelled with letters A to Y. Table 2 provides an overview with the computational settings and corresponding analytical parameter values calculated from Chézy's law and the strongly simplified second-order model of SOFD. We also used the fourth-order model, but we present the analytical results from the second-order model because they can easily be reproduced by the reader, For this second-order model, however, values of  $L_p$  can be calculated only in a limited range. A more complete fourth-order linear model (e.g. Zolezzi & Seminara, 2001) would have provided  $L_p$  values for other width-to-depth ratios in Table 2 too.

We compared the numerical results mainly with the results from linear analytical theories based on the same mathematical relations, in order to investigate the extent to which a fully non-linear model reproduces the predictions from linear models. A more thorough comparison with the experimental results of Zolezzi et al (2005) would have required more extensive calibration, involving the equifinality problem that different combinations of parameter values in the empirical closure relations may yield the same values of target quantities.

#### **4 RESULTS**

Figure 1 summarizes the results from all computations. The positive horizontal co-ordinates refer to the downstream straight reach and represent distances from the exit of the curved section. The negative horizontal co-ordinates refer to the upstream straight reach and represent distances from the entrance of the curved section. The bar heights plotted vertically have been calculated as half the difference between the bed level at the left bank and the right bank. The point of resonance is found to occur at  $\beta = 15$ , which is higher than the occurrence around  $\beta = 10$  predicted by the second-order linear model.

Furthermore, the computed bar wavelengths agree well with the values according to the linear model if  $\beta < 13$ , but they remain much shorter than their linear counterparts if  $\beta > 13$ .

Table 2 Overview of Delft3D simulations and corresponding analytical parameter values according to the SOFD second-order linear model

					Analytical results							
Run	<i>Q</i> (ℓ/s)	Δ <i>x</i> (m)	Δ <i>y</i> (m)	$\Delta t$ (s)	h <sub>0</sub> (m)	<i>u</i> <sub>0</sub> (m/s)	β	$\theta_0$	$\lambda_s / \lambda_w$	regime	$L_P$ (m)	
Α	42.80	0.10	0.03	0.03	0.097	0.735	3.1	0.647	0.23	sub		
В	20.00	0.20	0.06	1.50	0.058	0.570	5.1	0.390	0.49	sub	8.34	
C	10.50	0.20	0.06	1.50	0.038	0.460	7.9	0.254	0.93	sub	6.17	
D	8.06	0.20	0.06	1.50	0.032	0.421	9.4	0.213	1.22	sub	5.72	
Е	7.14	0.10	0.03	1.50	0.029	0.405	10.2	0.196	1.37	super	5.60	
F	7.00	0.20	0.06	1.50	0.029	0.402	10.3	0.193	1.40	super	5.58	
G	6.50	0.10	0.03	1.50	0.028	0.392	10.9	0.184	1.51	super	5.55	
Н	6.05	0.20	0.06	1.50	0.026	0.383	11.4	0.176	1.62	super	5.55	
I	5.90	0.20	0.06	1.50	0.026	0.380	11.6	0.173	1.66	super	5.56	
J	5.22	0.20	0.06	1.50	0.024	0.365	12.6	0.159	1.88	super	5.76	
K	4.60	0.20	0.06	1.50	0.022	0.350	13.7	0.146	2.13	super	6.42	
L	4.22	0.20	0.06	1.50	0.021	0.340	14.5	0.138	2.32	super	7.81	
M	4.02	0.20	0.06	1.50	0.020	0.334	15.0	0.134	2.44	super	10.04	
N	3.90	0.20	0.06	1.50	0.020	0.331	15.3	0.131	2.52	super	14.30	
О	3.70	0.20	0.06	1.50	0.019	0.325	15.8	0.126	2.65	super		
P	3.47	0.20	0.06	1.50	0.018	0.318	16.5	0.121	2.83	super		
Q	3.24	0.20	0.06	1.50	0.017	0.311	17.3	0.116	3.03	super		
R	3.02	0.20	0.06	1.50	0.017	0.304	18.1	0.110	3.25	super		
S	2.82	0.20	0.06	1.50	0.016	0.297	19.0	0.106	3.48	super		
T	2.64	0.20	0.06	1.50	0.015	0.290	19.8	0.101	3.72	super		
U	2.45	0.20	0.06	1.50	0.014	0.283	20.8	0.096	4.00	super		
V	2.15	0.20	0.06	1.50	0.013	0.271	22.7	0.088	4.56	super		
W	1.87	0.10	0.03	1.50	0.012	0.259	24.9	0.080	5.25	super		
X	1.75	0.10	0.03	1.50	0.012	0.253	26.0	0.077	5.61	super		
Y	1.66	0.10	0.03	1.50	0.011	0.249	27.0	0.074	5.91	super		

("sub" = subresonant, "super" = superresonant)

Figures 2 and 3 show the resulting bed topographies from runs J and X as representative examples from the subresonant and the superresonant regime. Non-migrating alternate bars occur only downstream of the curved section in the subresonant run J, and both upstream and downstream in the superresonant run X. In each run, forced spatial bars appeared at the entrance and exit of the curve almost immediately after the start of the simulation. Further away from the curved section, however, the regime was initially dominated by migrating bars. The bars in the downstream straight reach stabilized first by gradually decreasing their celerity. The upstream bars, if present, took longer to develop and stabilize. Rather than developing at the curve first and then expanding further upstream, they formed when migrating bars of a higher mode (i.e. with central bars, and even with more bars per cross-section in computations on a finer

grid for the highest values of  $\beta$ ) appeared at the upstream boundary, travelled downstream and stopped moving upon arrival at the entrance of the curve. They then retained their positions and transformed into a lower-mode pattern of alternate bars that gradually increased in length before attaining a final stable configuration.

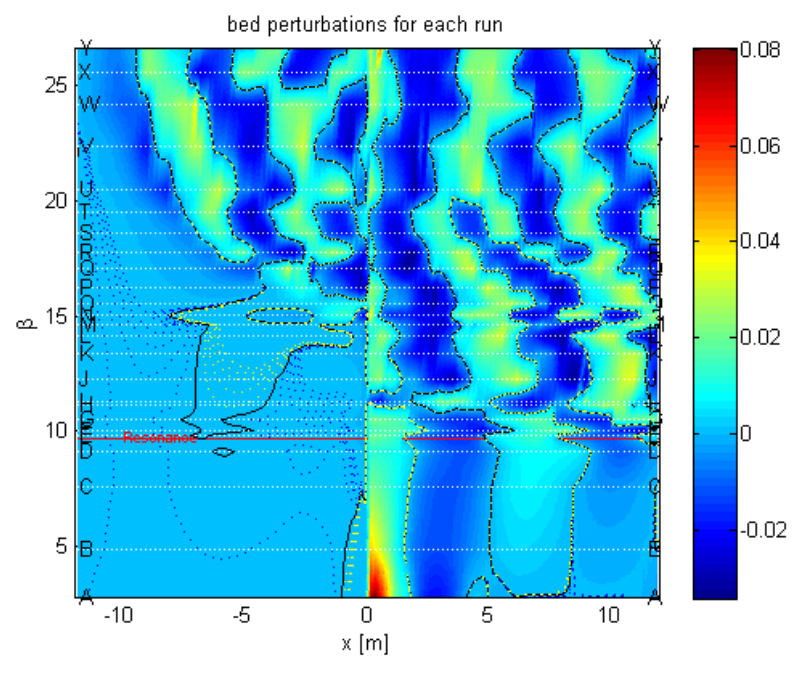


Figure 1 Summary of results from all simulations (runs A-Y): computed cross-sectional bed level differences as a function of distance from curved section in both upstream (negative co-ordinates) and downstream (positive co-ordinates) straight reaches

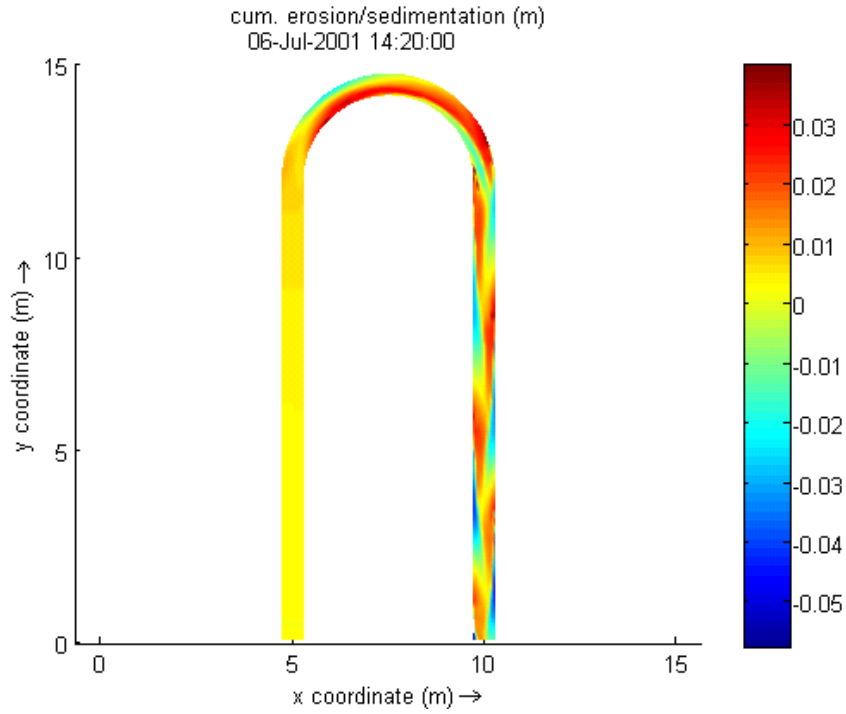


Figure 2 Simulation for subresonant parameter range: non-migrating bars and pools in straight reach only downstream of abrupt changes in channel curvature (Run J)

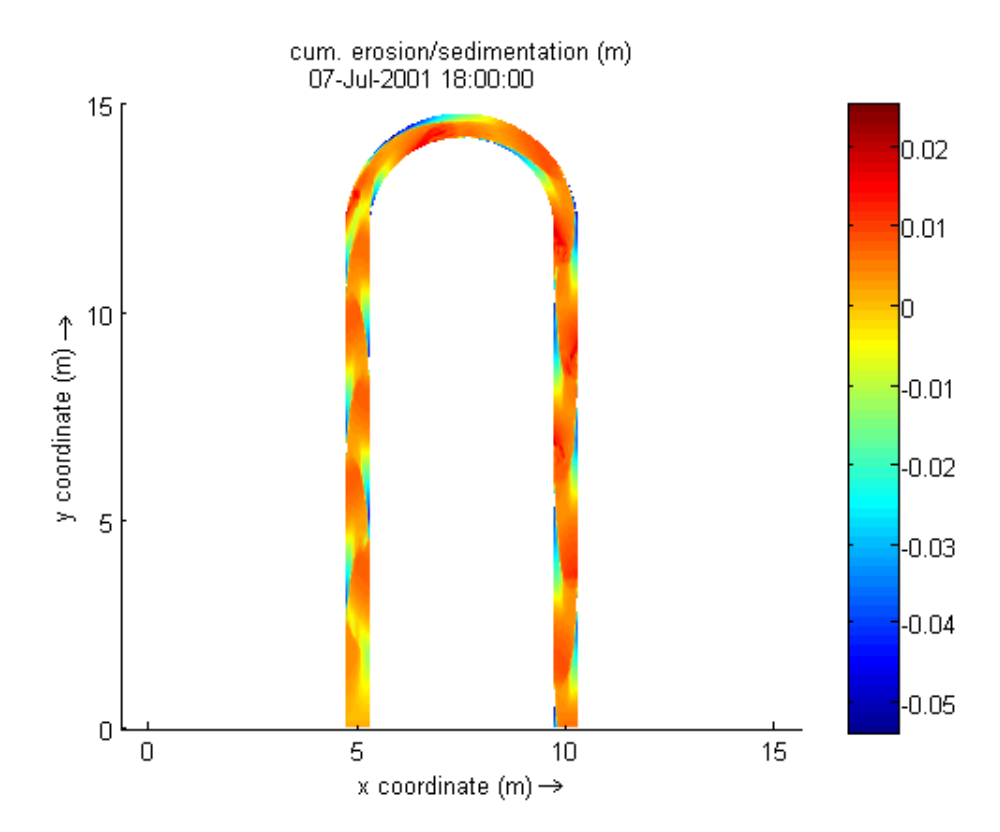


Figure 3 Simulation for superresonant parameter range: non-migrating bars and pools in straight reaches both upstream and downstream of abrupt changes in channel curvature (Run X)

#### 5 DISCUSSION

The results confirm numerically that the subresonant and superresonant morphodynamic regimes are markedly different. Non-migrating bars and pools appear downstream of geometrical perturbations if the regime is subresonant (Figure 2) and both upstream and downstream if the regime is superresonant (Figure 3). However, two findings in the computational results differ from linear theory and hence require closer investigation. First, the threshold between subresonant and superresonant regimes is higher in the numerical computations:  $\beta_{res} = 15$  instead of  $\beta_{res} = 10$ . Second, the non-migrating bars are significantly shorter than predicted by linear theory (and observed experimentally) if  $\beta > 13$ . We discuss possible explanations below.

The higher value of the threshold,  $\beta_{res}$ , between subresonant and superresonant regimes may be explained from numerical diffusion. This can be understood by realizing that the effect of transverse bed slopes on sediment transport direction has a diffusive effect too, which is demonstrated by substitution of Equation (1) without helical flow ( $\alpha_r = 0$ ) and without bed slopes in longitudinal direction ( $\partial z_b / \partial x = 0$ ) into the term for transverse sediment transport gradients in the sediment balance:

$$\frac{\partial q_{sy}}{\partial y} = \frac{\partial \left(q_{sx} \tan \alpha_s\right)}{\partial y} = \frac{\partial}{\partial y} \left(-\frac{q_{sx}}{f} \frac{\partial z_b}{\partial y}\right) = -\frac{\partial z_b}{\partial y} \frac{\partial}{\partial y} \left(-\frac{q_{sx}}{f}\right) - \frac{q_{sx}}{f} \frac{\partial^2 z_b}{\partial y^2}$$

$$\tag{6}$$

where  $q_{sx}$  and  $q_{sy}$  are the longitudinal and transverse components, respectively, of the sediment transport per unit width. The last term represents diffusion with a diffusion coefficient  $q_{sx}/f$ . The

diffusive character of the bed slope effect in the model implies that, conversely, numerical diffusion in the model alters the bed slope effect. Delft3D offers the possibility of using different numerical schemes for updating bed levels after erosion and sedimentation. For reasons of numerical stability, we used the standard first-order upwind scheme which exhibits numerical diffusion in longitudinal direction, but no numerical diffusion in transverse direction. However, as the flow winding around alternate bars has components in the directions of both longitudinal and transverse co-ordinates, numerical diffusion enters into the transverse components of the transport gradients in the sediment balance as well. Equations (2) and (3) show that a stronger effect of gravity pull along transverse slopes (smaller f, larger r) reduces the interaction parameter. A value apparently well above the resonant value can hence effectively be still below this value. We note that the fourth-order linear model predicts a higher  $\beta_{res}$  value than 10, but even that value is smaller than the value of 15 observed in the numerical results.

At least four explanations are possible for the shorter wavelengths at the highest width-to-depth ratios: (i) sediment stalling, (ii) limited simulation duration, (iii) numerical diffusion and (iv) nonlinear effects. We review each of these possible explanations below.

Sediment stalling (i) occurs when the bed shear stress exerted by the flow falls below the critical shear stress for incipient sediment motion. Even at the smallest discharges in our computations, however, the shear stresses remained well above this threshold. Hence sediment stalling has not played any role.

The importance of *simulation duration* (ii) has been demonstrated by the long-duration laboratory experiment and numerical computations of Crosato et al (2011). A pattern of non-migrating bars formed only after a very long time in straight channels without resonant width-to-depth ratio. Long durations were needed only in the absence of a geometrical perturbation. In situations with clear perturbations, the final pattern of non-migrating bars developed faster. Nonetheless, we observed in some of our computations that the bars were still in a process of becoming longer at the end of the simulation. The limited duration of our simulations hence might have contributed to finding shorter wavelengths.

The effect of *numerical diffusion* (iii) can be understood in the same way as for the higher value of  $\beta_{res}$ . The effective interaction parameter value is lower than the apparent value, and this corresponds to shorter bars. Numerical diffusion thus seems to offer a plausible explanation.

Evidence for shorter wavelengths due to *non-linear effects* (iv) is presented in the companion paper by Siviglia et al (2011). Their study suggests that an alluvial bed evolves into a non-migrating bar pattern with a wavelength that can be closer to that of spatial bars or that of migrating bars according to linear theory depending on the values of the half width-to-depth ratio,  $\beta$ , and the relative distance between the resonant value of the half width-to-depth ratio,  $\beta_{res}$ , and the critical value,  $\beta_{cr}$ , for the formation of free migrating bars. The wavelength becomes invariably shorter and closer to that of migrating bars, however, if the regime is superresonant, well away from the resonant width-to-depth ratio. The pattern tends to the wavelength of free alternate bars if the width-to-depth ratio becomes very large. This explanation seems plausible too.

Another observation in the numerical simulations is that the upstream overdeepening developed from free bars that migrated in downstream direction rather than the upstream direction expected for superresoant conditions. It is possible, however, that the higher-mode free bars were still in the subresonant regime, notwithstanding the superresonant conditions for the first-mode alternate bars. Moreover, the theoretically predicted upstream migration of free bars in the superresonant regime applies only when their amplitude is small, as the upstream-migrating bars have a much smaller temporal growth rate than their downstream-migrating counterparts.

#### 6 CONCLUSIONS

Our numerical computations confirm the essential differences between the subresonant and the superresonant regime. However, the threshold between the two regimes is higher than predicted by linear theory, and, at high width-to-depth ratios in the superresonant regime, the non-migrating bars and pools are shorter than predicted by linear theory (and shorter than observed experimentally too). We explain the higher threshold from numerical diffusion, and the shorter bars from limited simulation duration, numerical diffusion and non-linear effects. More research is needed to quantify the individual contribution of each of the possible causes identified.

## REFERENCES

- Blondeaux, P. & Seminara, G., 1985, A unified bar-bend theory of river meanders. J. Fluid Mech., vol.157, pp.449-470.
- Callender, R.A., 1969, Instability and river channels. Journal of Fluid Mechanics, Vol.36, Part 3, pp.465-480.
- Camporeale, C., Perona, P., Porporato, A. & Ridolfi, L., 2007, Hierarchy of models for meandering rivers and related morphodynamic processes. Rev. Geophys., 45, RG1001, doi:10.1029/2005RG000185.
- Colombini, M., Seminara, G & Tubino, M., 1987, Finite-amplitude alternate bars. J. Fluid Mech., vol.181, pp.213-232.
- Crosato, A., 1989, Meander migration prediction. Excerpta, GNI, Vol.4, Libreria Progetto, Padova, pp.169-198.
- Crosato, A., 2008, Analysis and modelling of river meandering. PhD thesis, Delft University of Technology, IOS Press, ISBN 978-1-58603-915-8.
- Crosato, A., Mosselman, E., Beidmariam Desta, F. & Uijttewaal, W.S.J., 2011, Experimental and numerical evidence for intrinsic nonmigrating bars in alluvial channels, Water Resources Research, Vol.47, W03511, doi:10.1029/2010WR009714.
- Engelund, F. & Hansen, E., 1967, A monograph on sediment transport in alluvial streams. Teknisk Forlag, Copenhagen. Hansen, E., 1967, On the formation of meanders as a stability problem. Progress Rep. 13, Coastal Engrg. Lab., Tech. Univ. of Denmark, Basic Res., pp.9-13.
- Lesser, G.R., Roelvink, J.A., Van Kester, J.A.T.M. & Stelling, G.S., 2004, Development and validation of a three-dimensional morphological model. Coastal Engrg., Vol.51, Nos.8-9, pp.883-915.
- Meyer -Peter, E. & Müller, R., 1948, Formulas for bed-load transport. Proc. 2nd Congress IAHR, Stockholm, Paper No.2, pp.39-64.
- Mosselman, E., 2005, Basic equations for sediment transport in CFD for fluvial morphodynamics. Chapter 4 in: Computational Fluid Dynamics; Applications in environmental hydraulics, Eds. P.D. Bates, S.N. Lane & R.I. Ferguson, Wiley, pp.71-89.
- Mosselman, E., Tubino, M. & Zolezzi, G., 2006, The overdeepening theory in river morphodynamics: Two decades of shifting interpretations. Proc. River Flow 2006, Lisbon, 6-8 Sept., 2006, Eds. R.M.L. Ferreira, E.C.T.L. Alves, J.G.A.B. Leal & A.H. Cardoso, Publ. Taylor & Francis, London, ISBN 978-0-415-40815-8, Vol.2, pp.1175-1181.
- Parker, G & Johanneson, H. 1989, Observations on several recent theories of resonance and overdeepening in meandering channels. In: River meandering, AGU, Water Resources Monograph 12, Eds. S. Ikeda & G. Parker, pp.379-415.
- Siviglia, A., Vanzo, D., Stecca, G., Tubino, M. & Zolezzi, G., 2011, Interaction between steady and migrating bars in straight channels. Proceedings RCEM 2011, Beijing, China, September 6-8, 2011.
- Struiksma, N., Olesen, K.W., Flokstra, C. & De Vriend, H.J., 1985, Bed deformation in curved alluvial channels. J. Hydr. Res., IAHR, Vol.23, No.1, pp.57-79.
- Talmon, A.M., Struiksma, N. & Van Mierlo, M.C.L.M., 1995, Laboratory measurements of the direction of sediment transport on transverse alluvial-bed slopes. J. Hydr. Res., IAHR, Vol.33, No.4, pp.495-517.
- Zolezzi, G & Seminara, G 2001. Downstream and upstream influence in river meandering; Part 1, General theory and application to overdeepening. J. Fluid Mech., 438: 183-211.
- Zolezzi, G, Guala, M., Termini, D., Seminara, G 2005. Experimental observations of upstream overdeepening. J. Fluid Mech., 531: 191-219.